Theoretical and Applied Fracture Mechanics 116 (2021) 103109

Contents lists available at ScienceDirect

Theoretical and Applied Fracture Mechanics

journal homepage: www.elsevier.com/locate/tafmec

Optimal shot peening residual stress profile for fatigue

S. Aguado-Montero *, J. Vázquez, C. Navarro, J. Domínguez

Departamento de Ingeniería Mecánica y Fabricación, Universidad de Sevilla, Camino de los Descubrimientos s/n, C.P 41092, Sevilla, Spain

ARTICLE INFO

Keywords:
Residual stress
Shot peening
Optimization
Fatigue crack growth

ABSTRACT

Shot peening (SP) is frequently used as a palliative measure against metal fatigue in many engineering components. The performance of this surface treatment depends on different factors including the material, shape and loading conditions of the component, as well as process parameters. Fatigue improvement due to SP depends to a great extent upon the in-depth compressive residual stress profile produced in the specimen.

In this work, we study the optimum shape for a residual stress profile in terms of fatigue behaviour. For this task, we assume a residual stress profile that is qualitatively similar to that produced by SP in many metals. Based on this generic profile, we analyse the optimum shape for two simple, but noteworthy, fatigue cases: plain fatigue and notch fatigue. The analysis is conducted in the ''fatigue damage tolerance design'' framework, in which a certain initial defect is assumed to be present in the component under study.

1. Introduction

Fatigue is a material damage phenomenon that is present in many engineered metallic components. It occurs when components are subjected to time-fluctuating loads, and its most recognizable effect is the appearance of cracks, which, under suitable conditions, can propagate until the complete fracture of the component, thus causing catastrophic failure in some cases. Due to this potential risk of component failure, many palliatives are used in order to mitigate, or even eliminate, the fatigue process. Shot peening (SP) is widely used as a surface treatment in order to improve fatigue performance in a wide variety of metals and situations [1,2]. Its widespread use in the mechanical industry can be explained by the noticeable enhancement in fatigue behaviour of most metals, its relatively low price and its ease of use in the majority of engineering components. Its most attributable and recognizable effect is to produce an in-depth compressive residual stress field but also a substantial modification of the surface roughness and the near-surface material hardness [3,4].

As a rule of thumb, it can be said that SP process parameters depend on the particular application, i.e., the raw material and type of loading applied to the treated component. For a certain material, these process parameters define the shape of the in-depth residual stress profile. The SP industry has a long history and wide experience in selection of appropriate parameters for a certain application, but in the majority of cases this is based on a phenomenological experience and, to the best of the authors' knowledge, no analysis concerning how the SP-induced residual stress profile produced with a particular set of parameters modifies fatigue behaviour has been conducted in the past.

Shot peening residual stress profiles are known to adopt a specific type of spatial configuration which is termed the *sinusoidal decay function*, as described in [5]. Section 2 is dedicated to the analysis of the main aspects concerning the sinusoidal decay function. From the designer's point of view, the following difficult questions arise: for a particular application, which is the optimum shot peening residual stress profile? Is there a residual stress field that, following a sinusoidal decay function scheme, maximizes fatigue strength of the specimen? It is important to define a metric for the optimality of a residual stress profile, i.e. fatigue strength needs to be properly defined before it is maximized.

For a typical metallic specimen, fatigue life is composed of two substantially different stages: crack initiation and propagation. Each of these phases involves very distinct physical processes, resulting in the need for different mathematical models to properly capture the whole specimen's fatigue life. While crack initiation life is mainly governed by local stresses in the vicinity of the crack initiation site, crack growth is controlled by the stress intensity factor, a magnitude that depends on both the stress level in the region where the crack is developing and the geometry of this cracked region itself.

From a crack initiation point of view, compressive residual stresses would lower the stress levels at the crack initiation location, turning crack formation into a more unlikely event. From a fatigue crack propagation perspective, the presence of these compressive residual stresses would result in smaller stress intensity factors associated to the crack evolution, slowing down or even stopping the process.

* Corresponding author.
E-mail address: saguado@us.es (S. Aguado-Montero).

https://doi.org/10.1016/j.tafmec.2021.103109
Received 1 June 2021; Received in revised form 6 September 2021; Accepted 14 September 2021
Available online 20 September 2021

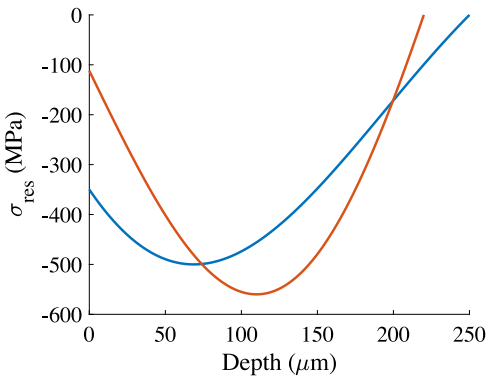

Fig. 1. Two different residual stress configurations.

For these reasons, residual stress configurations achieving higher compression are expected to perform better. However, it is not that clear how those residual stresses should be distributed within the specimen's domain. Should higher compressive stresses be present immediately adjacent to the free surface, or should they be located at deeper positions so as to be able to affect a more general volume? If initiation life were to be considered as the main contribution to fatigue life, stresses in the vicinity of the initiation site would need to be minimized. If one considers that crack initiation usually takes place at some point of the specimen's surface, then crack initiation life could be maximized by adopting a residual stress profile where maximum compressions are applied right next to the specimen's surface, in a region that is usually denoted as the process zone, where initiation takes place. On the contrary, if fatigue crack growth life is considered to be the main contribution to the specimen's fatigue life, the residual stress profile should be strategically designed in such a way that provides the stress intensity factors that result in the slowest possible fatigue crack growth. A situation where stress intensity factor took values below the crack growth threshold would be of particular interest, since fatigue crack growth would be completely stopped and fatigue crack growth life would become infinite.

The problem of selecting a proper residual stress profile is sketched in Fig. 1, in which two typical SP residual stress distributions are plotted; the material is assumed to be a type of steel with a yield limit, σ_y, of about 800 MPa. In addition, to simplify the discussion, it is assumed that the potential crack mouths will be subjected to a constant amplitude loading. In this image, it is clear that for cracks smaller than about 75 μm the residual stress distribution with higher compressive stresses near the surface, depicted in blue, will behave better against fatigue; however, for cracks between 75 μm and 200 μm, the residual stress profile that provides higher compressive stresses at depths ranging from 75 to 200 μm, depicted in orange, might be expected to perform better since higher compressive stresses close to the crack tip might be able to delay or stop crack growth. Finally, it is not easy to predict the best profile for cracks longer than 200 μm, so a complete analysis needs to be taken into consideration. The overall fatigue behaviour will depend on the evolution of the mode I stress intensity factor range, ΔK_I, and also – if a Paris type crack growth law is considered – on the m exponent.

In the present work, we consider a situation where a previously generated defect is present in the specimen's domain. This condition can represent some type of manufacturing imperfection as the ones found in metal welding or additive manufacturing. This already existing defect can act as a crack whose initiation life can be neglected, thus considering that it will start propagating right away, resulting in fatigue crack growth life of this specimen being equal to its complete fatigue life since the defect already exists and no crack initiation life needs to be taken into account. This kind of analysis is usually termed "fatigue damage tolerant design" and is of practical interest in disciplines such as the aforementioned metal welding and additive manufacturing, as well as gas turbine blade design. Moreover, fatigue damage tolerant design provides the opportunity to focus exclusively in the fatigue crack growth phase, resulting in a simpler and more comprehensive analysis, with fewer parameters and variables involved.

Now that the problem has been simplified to a point where only fatigue crack growth life is to be calculated, it is possible to define fatigue strength: for those situations where cracks can grow from its initial state to final failure of the specimen, fatigue strength equals fatigue crack growth life; if the crack is arrested at some point during its growing process, if applied loads are not high enough, then fatigue crack growth becomes infinite and fatigue strength is defined as a measure of the robustness of the specimen, i.e. the perturbation required for the crack to grow up to final failure. The higher the overload or perturbation needed to make the crack grow, the higher the fatigue strength associated to the specimen. Section 3 deals with the mathematical details of fatigue strength quantitative analysis.

Furthermore, and assuming that the shape of the shot peening induced residual stress profile can be properly described with a *sinusoidal decay function*, a new set of more comprehensive parameters is first proposed, and then a nondimensional analysis is developed for the problem. In this way, we try to obtain the optimum value for the parameters governing the sinusoidal decay function, thus maximizing the component's fatigue strength.

There are only a few works in the bibliography that attempt to obtain the optimal residual stress configuration for strength against fatigue, but only shot peening process parameters are investigated: not the residual stress profile producing the best performance [6,7]. In the present work we analyse the optimum residual stress profile, based on the *sinusoidal decay function*, in two simple, but noteworthy, fatigue cases: plain fatigue and notch fatigue. In the approach followed here, it is assumed that the component has an initial crack which, for the sake of simplicity, is assumed to be perpendicular to the component surface. According to this, only the fatigue crack growth phase is analysed. In addition, only surface through cracks are considered. Furthermore, it is assumed that the fatigue crack growth follows the Paris crack growth law. All of these elements lead to a significant reduction in the number of parameters involved in the problem, thus making the analysis possible and also more comprehensive. Despite these required simplifications, the analysis performed here can be of great interest because cracks nucleate at the surface in many actual situations – either by fatigue or some manufacturing process – and then propagate nearly perpendicularly to the surface. Also, many surface cracks are more or less semi-elliptical and shallow, thus having a mode I stress intensity factor very close to that of a through crack. Finally, it is well known that the Paris equation is suitable for region II (the linear zone in the log–log plot of the $\frac{da}{dN} - \Delta K$ sigmoidal curve), but extrapolating it to region I (the near threshold zone) can be either conservative or non-conservative: moreover, extrapolating it to zone III (the fast crack growth region) produces non-conservative predictions due to the sigmoidal shape of the $\frac{da}{dN} - \Delta K$ curve. However, the crack growth life spent in region III is very small as compared to that in zones I and II, and thus the integration of the Paris crack growth law over zones I, II and III may be reasonable in many situations.

2. Mathematical modelling of a residual stress profile

A systematic analysis of residual stress profiles produced by shot peening has been taken into consideration several times in the recent literature, making use of the *sinusoidal decay function*, as can be observed in [5] and [8]. In a sinusoidal decay function analysis, the number of coefficients to fit is always constant, namely 4:

$$\sigma_{res}(z) = Ae^{-\lambda z}\cos(\omega z + \theta) \tag{2.1}$$

where A, λ, ω and θ are the aforementioned coefficients that control the shape of a general residual stress profile and z measures depth from the specimen's surface. Eq. (2.1) models the compressive fraction of the residual stress profile, so it is defined only from $z = 0$ to a depth where $\sigma_{res} = 0$. The main benefit of this methodology is its ease of use, as opposed to a common polynomial fit, which can become arbitrarily complex as the degree of the function grows [8].

However, these coefficients do not allow for a straightforward understanding of the shape of the curve since they do not have a direct physical counterpart; i.e. if the values of these four parameters are known, then a sketch of the residual stress profile is required to draw any conclusion about it. The coefficients on their own are not sufficient to qualitatively imagine the main aspects of the curve. As a solution to this issue, a new set of parameters is proposed:

- σ_0 represents the absolute value of the stress level at the specimen's surface.
- z_0 controls the location where the residual stress profile transitions from a compressive situation to a tensile regime, i.e. the size of the compressive residual stressed region.
- σ_{max} denotes the maximum absolute value of the residual stress profile.
- z_{max} points to the location where σ_{max} takes place.

How the new set of parameters completely describes the shape of the curve can be readily determined, simplifying the analysis of the problem.

The next steps in the process involve relating both sets of parameters and also constructing a nondimensional version of the sinusoidal decay function. If the Π Buckingham theorem is taken into consideration, Eq. (2.1) involves 6 magnitudes with only 2 different dimensions (length and stress), which means that the relation of 4 nondimensional variables can be obtained. This observation remains true if the new set of parameters is used since the number of both magnitudes and dimensions are unchanged. Appendix A explains in detail how the following expression is obtained:

$$\frac{\sigma_{res}}{\sigma_{max}} = \frac{Ae^{-\lambda z}\cos(\omega z + \theta)}{Ae^{-\lambda z_{max}}\cos(\omega z_{max} + \theta)} \tag{2.2}$$

Taking into consideration the relations existing between both sets of parameters developed in Appendix A,

$$\theta = \theta\left(\frac{z_{max}}{z_0}, \frac{\sigma_0}{\sigma_{max}}\right); \quad \lambda = \lambda\left(\frac{z_{max}}{z_0}, \frac{\sigma_0}{\sigma_{max}}\right); \quad \omega = \omega\left(\frac{z_{max}}{z_0}, \frac{\sigma_0}{\sigma_{max}}\right) \tag{2.3}$$

The combination of Eqs. (2.2) and (2.3) yields the following qualitative expression:

$$\frac{\sigma_{res}}{\sigma_{max}} = \frac{\sigma_{res}}{\sigma_{max}}\left(\frac{z}{z_0}, \frac{\sigma_0}{\sigma_{max}}, \frac{z_{max}}{z_0}\right) \tag{2.4}$$

From now on, nondimensional variables appearing in Eq. (2.4) will be denoted as the numerator followed by a '*' sign, namely σ^*_{res}, z^*, σ^*_0 and z^*_{max}, to simplify notation.

Eq. (2.4) cannot be defined in the whole (z^*_{max}, σ^*_0) domain. As discussed in Appendix A, the numerically consistent domain is mainly restricted by the relation $z^*_{max} < 0.545$. This means that the sinusoidal decay function is not able to model a compressive residual stress profile whose extreme value is deeper than approximately half its size, z_0.

3. Optimization criteria

As posed in the introduction, initiation of cracks will not be taken into consideration in the present work. This means that the presence of a previously initiated surface crack (or perhaps a crack-like defect present in the specimen) of length a_i is assumed, thus enabling exploration of the 'fatigue damage tolerance design' framework.

Crack evolution will be studied via integration of a Paris type crack growth law, defined by two coefficients, C and m (as a first analysis, neither the crack growth threshold nor crack closure will be considered).

$$\int_0^{N_f} dN = \int_{a_i}^{a_f} \frac{da}{CK^m} \tag{3.1}$$

Integration of a Paris type crack growth law, in order to obtain crack propagation life, is shown in Eq. (3.1). This integration is considered from the initial state of the defect until a crack length such that the tip of the crack falls outside the compressive residual stressed region, i.e., depth z_0. This simplification is supported by the idea that crack growth will be much faster once the crack tip enters the tensile residual stress domain, hence reaching failure in a significantly smaller amount of cycles than that required to reach from the initial state to depth z_0. Appendix B explains in detail how this integration is calculated and explores a procedure to obtain a nondimensional result for both stress intensity factors and fatigue crack growth life. Stress intensity factors are calculated as follows:

$$K(a) = \int_0^a \sigma(z)\, w(z, a)\, dz \tag{3.2}$$

where σ is the applied stress and w denotes the weight function. To clarify concepts, let us denote by N^* the specimen's fatigue crack growth life in the presence of a particular residual stress profile divided by the same variable calculated without taking residual stresses into account, i.e. nondimensional fatigue crack growth life measures the improvement in fatigue strength for the specimen due to the presence of a certain residual stress configuration. Eq. (3.3), which is explained in detail in Appendix B, shows the ratio between the fatigue crack growth life in the presence of a particular residual stress configuration and the fatigue crack growth life in a situation free from residual stress.

$$N^* = \frac{\int_{a^*_i}^1 ((K^*_{res} + K^*_{applied})\sqrt{a^*})^{-m}\, da^*}{\int_{a^*_i}^1 (K^*_{applied}\sqrt{a^*})^{-m}\, da^*} \tag{3.3}$$

where $a^*_i = \frac{a_i}{z_0}$, $a^* = \frac{a}{z_0}$ and K^* is the stress intensity factor adimensionalized by the reference value $1.12\sigma_{max}\sqrt{\pi a}$. This reference value is defined as the stress intensity factor associated to a semiinfinite domain containing a superficial through crack of length a, subjected to a remote uniform reference stress level σ_{max}. Note how N^* is a function of initial crack length a_i, Paris crack growth law exponent m, applied loads and geometry.

Now that the main variables governing the problem have been established, it is necessary to define the optimality criteria. The main goal is to maximize the specimen's strength for a given initial defect. Fig. 2 summarizes the following analysis in the form of a flowchart. For every situation that is to be analysed, the following question needs to be answered: Is there any residual stress configuration that produces a negative stress intensity factor for some crack length ranging from initial crack length a_i to final length z_0? If the answer is negative, then the crack will eventually outgrow the residual stressed region and this will be considered as a catastrophic failure. In this situation, the optimum residual stress profile will be chosen as the one that maximizes the specimen's fatigue crack growth life until failure. In the opposite case; i.e., if there exists at least one residual stress profile that produces a negative stress intensity factor (not necessarily at the initial crack length: it can be anywhere from the initial state to a depth z_0), then the optimum residual stress configuration is the one that minimizes the stress intensity factor for some crack length in the range from a_i to z_0. This can be imagined as building the highest possible barrier for the crack, preserving the specimen from any kind of unexpected perturbation that could slightly decrease its theoretical strength. It is important to note that we are not minimizing the stress intensity factor for the initial crack length, but rather allowing for this minimum stress intensity factor to occur at any crack length from a_i to z_0. This means that a situation in which the stress intensity factor is positive in the original state (thus making the crack grow) is perfectly possible, but

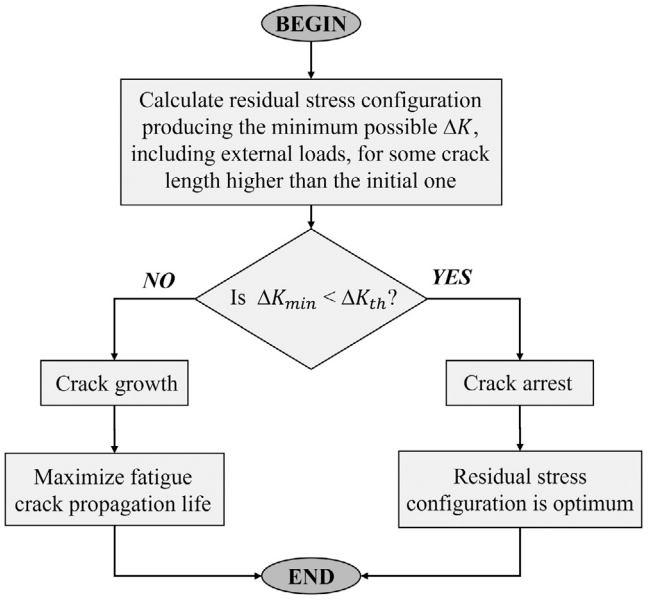

Fig. 2. Optimization criteria flowchart.

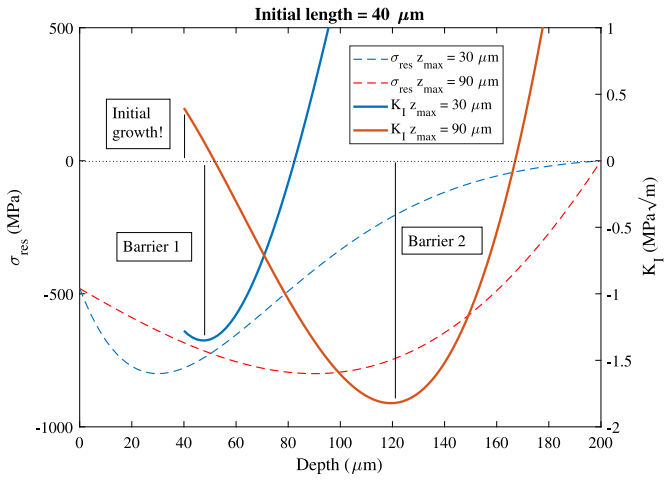

Fig. 3. Two examples of residual stress configurations and resulting mode I stress intensity factors.

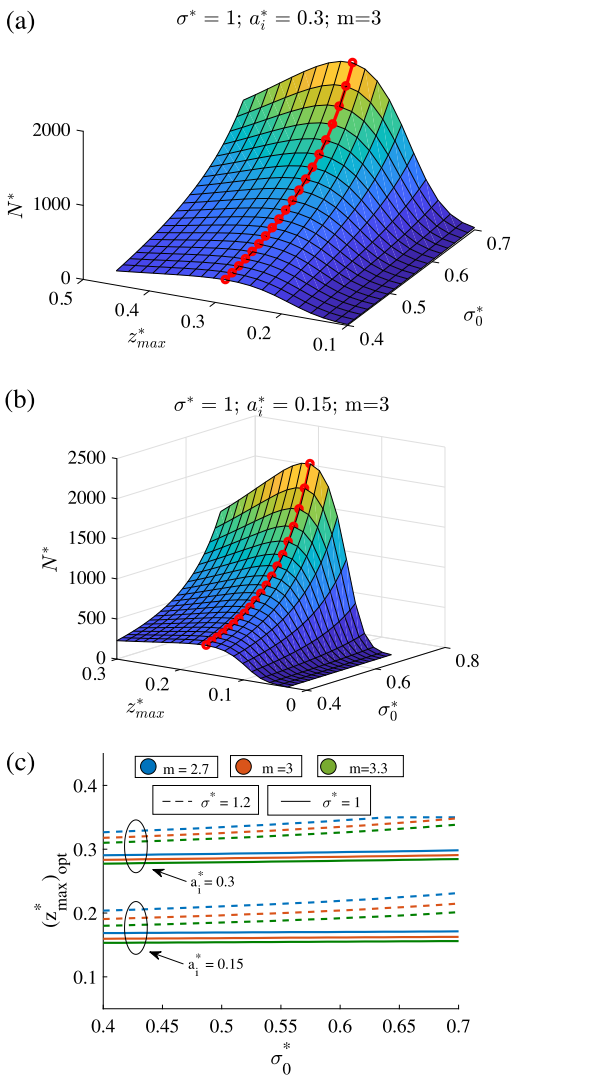

Fig. 4. (a)(b) Nondimensional fatigue crack growth life as a function of the nondimensional residual stress profile parameters for two different initial crack lengths. Marginal maximum values with respect to z^*_{max} are also included as a dotted red line, showing no dependence upon σ^*_0 or m, but clear variability with a_i^*. (c) Optimum solution for z^*_{max} as a function of σ^*_0, for different values of m, a_i^* and σ^*, in the finite life regime.

the crack will eventually reach the aforementioned barrier, which is the highest possible barrier that could be present, thus minimizing the probability of the crack exceeding this point and reaching the tensile residual stress domain. In other words, no life optimization is obtained in this case because life is infinite, and no failure will take place.

Fig. 3 shows an example of this situation in which no catastrophic failure will take place. The situation considered is as follows: applied stress (uniform) is $\sigma = 640$ MPa, maximum residual stress is $\sigma_{max} = 800$ MPa, superficial residual stress is $\sigma_0 = 480$ MPa and residual stresses become zero at depth $z_0 = 200$ μm. The initial defect has a length of $a_i = 40$ μm and both solid curves represent stress intensity factor evolution as the crack increases its length for two different residual stress maximum locations z_{max}. It is clear that both of the residual stress configurations will stop the crack at some point since both of them adopt negative K_I values. More precisely, the configuration depicted in blue ($z_{max} = 30$ μm) will not allow the crack to grow at all, whereas the other configuration, depicted in red ($z_{max} = 90$ μm), would allow the crack to grow a distance of about 10 μm before causing it to stop. From this perspective, the first configuration might seem better, but if one considers a slight perturbation in the system, then the second one is more robust due to its smaller minimum, thus preventing the crack from ever developing beyond the compressive residual stressed domain. For this reason, this second configuration will be considered as closer to the optimum solution for this type of situation in which cracks do not grow to complete failure.

4. Plain fatigue

In this section, a semi-infinite plain specimen, containing a superficial through crack of length a_i subjected to uniform constant amplitude remote load σ, is analysed (the loading ratio $R = -1$ is considered throughout the whole paper). The main goal is to provide sufficient information so as to choose the optimum residual stress profile for the specimen, i.e. the values of the nondimensional variables σ^*_0 and z^*_{max}. Notice how applied stress can be nondimensionalized as follows: $\sigma^* \equiv \frac{\sigma}{\sigma_{max}}$.

Consider the results shown in Figs. 4a and 4b, where nondimensional fatigue crack growth life (i.e. the specimen's fatigue crack growth life improvement due to the presence of a certain residual stress profile) is plotted as a function of the optimization variables for two different

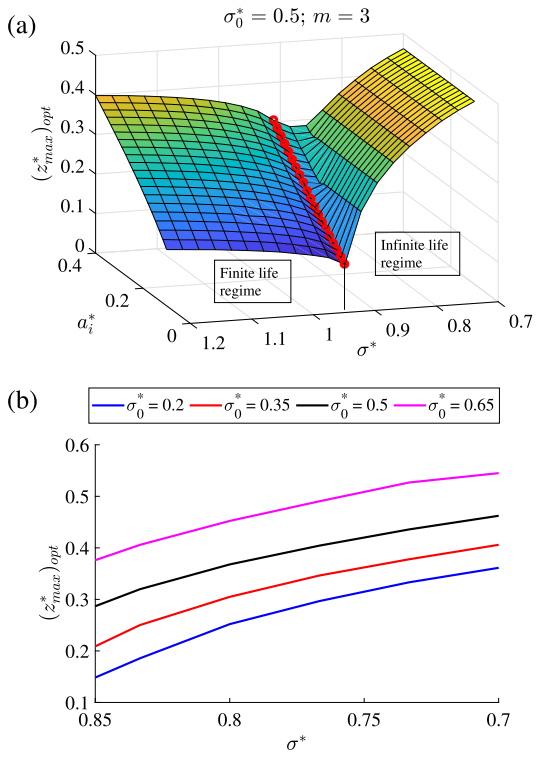

Fig. 5. (a) Optimum solution for z^*_{max} in both finite and infinite life regimes, separated by red line; (b) Optimum solution for z^*_{max} as a function of σ^* in the infinite life regime for different values of parameter σ_0^*.

initial crack lengths in a situation where cracks do grow until final failure, so that fatigue crack growth life can be optimized. Notice how initial crack length can be nondimensionalized as $\frac{a_i}{z_0} \equiv a_i^*$. The black grid that is displayed on top of the surfaces represents the numerically simulated data. A simulation was considered at every intersection point between two black lines. A 20×20 numerical simulation grid was used. A similar procedure was considered in Figs. 5a, 6a, 6b, and 7.

It can be observed that the shapes of the surfaces in Figs. 4a and 4b follow similar trends

- As one increases σ_0^*, N^* always increases, regardless of z^*_{max}.
- If σ_0^* is kept constant and z^*_{max} is modified, then a local maximum can be found, so there actually exists an optimum value for z^*_{max} that maximizes the specimen's fatigue crack growth life for a particular σ_0^* value.
- The value at which $(z^*_{max})_{opt}$ is found does not significantly depend on σ_0^*, but it does depend on the initial length of the crack a_i^*.

These three considerations suggest that both optimizing variables σ_0^* and z^*_{max} can be separated, thus accomplishing two independent single variable optimizations. Furthermore, optimization with respect to σ_0^* is straightforward since a higher stress level at the specimen's surface corresponds with greater strength improvement, so σ_0^* should remain as high as technically possible in the finite life regime. Fig. 4c shows a notable dependence on a_i^* for the optimum z^*_{max} values, a limited dependence on σ^* and marginal variation with respect to m and σ_0^*.

Let us now focus on computing the optimum value for z^*_{max} for a given set of parameters a_i^*, σ^*, σ_0^* and Paris law coefficient m. For a first analysis, a_i^* is expected to be an important parameter, as shown by Figs. 4a and 4b, as well as is σ^* since it will mainly control the transition from finite to infinite life regime. σ_0^* has been shown to exert very little influence on z^*_{max}, at least in the finite life regime, so its effects will be analysed later on, just as with Paris law coefficient m.

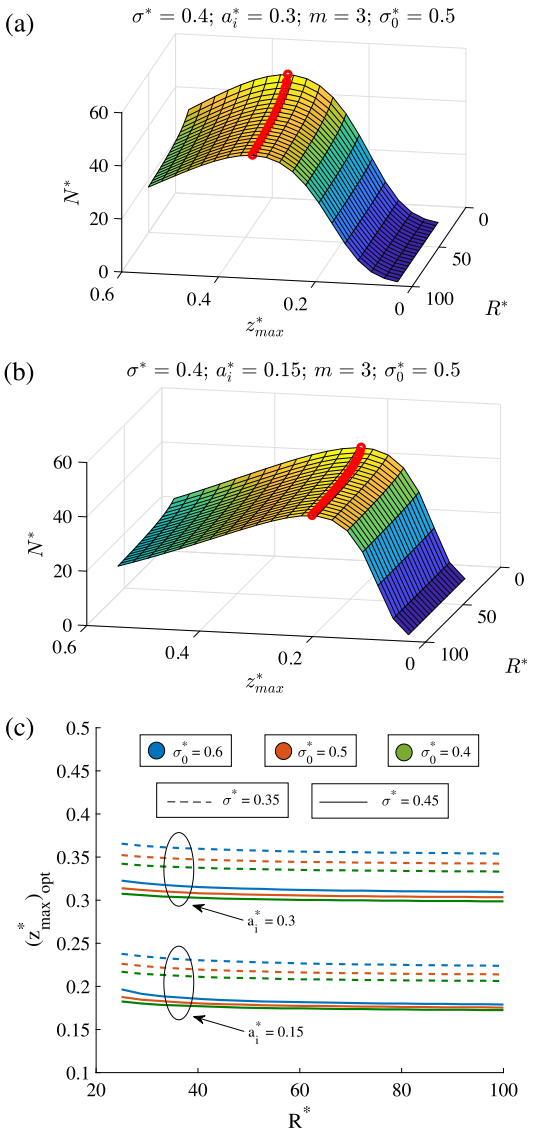

Fig. 6. (a) (b) Nondimensional fatigue crack growth life as a function of z^*_{max} and R^* for two different initial crack lengths. Marginal maximum values with respect to z^*_{max} are also included as a dotted red line, showing no dependence upon R^*, but a clear variability with respect to a_i^*. (c) Evolution of z^*_{max} with respect to R^* for several values of σ_0^*, σ^* and a_i^* in the finite life regime.

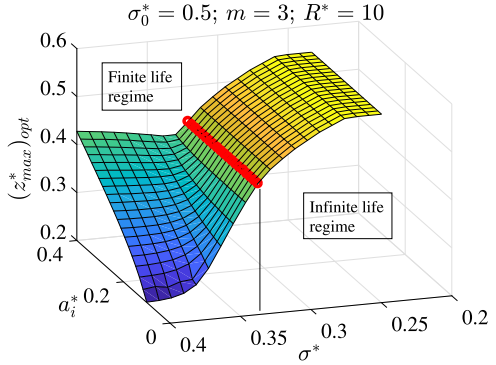

Fig. 7. Optimum solution for z^*_{max} in the notch fatigue case for a certain R^* value. Finite and infinite life regimes are separated by a red line.

Fig. 5a shows optimization results for z^*_{max} as a function of a^*_i and σ^*, keeping σ^*_0 and m as fixed parameters. It is important to notice the red line that splits the surface into two different parts. For remote stress levels above $\sigma^* \approx 0.95$ (left hand side of the diagram), cracks are able to grow until final failure, so finite life optimization is considered, maximizing the specimen's fatigue crack growth life. On the contrary, for remote stress levels below $\sigma^* \approx 0.95$ (right hand side of the diagram), cracks are not able to grow until failure because they face a negative stress intensity factor at some point, so an infinite life optimization has been implemented, minimizing the stress intensity factor for some crack length ranging from initial crack length a_i to z_0.

The finite life region (left hand side of the diagram) shows little dependence on σ^* and instead varies almost linearly with initial crack length a^*_i. This is coherent with Figs. 4a and 4b, where important differences were observed as a^*_i was modified. As a general rule of thumb, it can be observed that the maximum residual stress location tends to follow the initial crack tip.

The infinite life region (right hand side of the diagram) exhibits completely different behaviour. In this situation, almost no dependence was observed with respect to a^*_i, but instead σ^* is now the governing variable. Dependence with respect to Paris law exponent m was not observed in any of the situations (the infinite life region could not depend on m since no crack growth is considered), so it can be readily retained as a constant with reference value $m \approx 3$ without loss of generality. In the case of σ^*_0, no variation was expected in the finite life regime, as exhibited in Figs. 4a and 4b, but a substantial effect was produced in the infinite life region. Due to the fact that no a^*_i dependence is observed in this region, results were projected in the $z^*_{max} - \sigma^*$ plane and shown in Fig. 5b for several σ^*_0 values. Notice how the different curves obtained follow very similar trends. As σ^*_0 increases, the optimum solution for z^*_{max} is shifted towards higher values.

5. Notch fatigue

In this section, the previous plain fatigue analysis is generalized to a situation in which a circular notch, with radius R, is present in the specimen's domain. For this configuration, cracks are expected to initiate in the symmetry plane due to the well-known stress concentration factor of 3 occurring at the root of the notch. From now on, the z coordinate will be measured from this very root of the notch, not from the original free surface. Additionally, notch radius R is nondimensionalized with z_0, and thus $R^* \equiv \frac{R}{z_0}$.

The first difference to be noticed with respect to the plain fatigue situation is that an extra parameter, R^*, is included in the analysis for this geometry. Fig. 6a–6b show how nondimensional life, N^*, varies with z^*_{max} and R^* in the finite life regime, in a similar manner as in Fig. 4a–4b in the plain fatigue case, but substituting σ^*_0 for the new variable, R^*. This can be done without loss of generality since it has been shown how σ^*_0 exerts almost no effect as long as the crack is able to grow. Indeed, the same conclusion can be drawn from Fig. 6a–6b since $(z^*_{max})_{opt}$ is observed to be almost independent of R^* in the finite life regime, whereas the initial crack length a^*_i notably impacts the optimization results, according to Fig. 6c. For these reasons, $(z^*_{max})_{opt}$ will now be studied as a function of a^*_i and the remote stress level σ^*. The infinite life regime will also be analysed, where dependencies with respect to R^* and σ^*_0 are expected to exist.

Fig. 7 is the direct counterpart of Fig. 5a for a certain R^* value in the notched fatigue case. Even though the surface appears to be quite similar to the plain fatigue situation, two major differences can be found when a deeper analysis is taken into consideration.

On the one hand, the minimum stress level required to make cracks grow, i.e. transitioning stress level σ^* from infinite to finite life regimes, shows a significant dependence on notch dimension R^*, as can be found in Fig. 8. It can be readily determined that as R^* tends to infinity, stress gradients are negligible and we recover the plain fatigue situation (with remote stress levels divided by a factor of three, due to the stress concentration factor). For smaller R^* values, the remote stress level required to make cracks grow increases, thus restricting the finite life regime. It can be argued that this is the reason why R^* shows no effect over $(z^*_{max})_{opt}$ in the finite life regime: this can only happen if R^* takes a rather large value, so stress gradients are not significant and we recover once again the plain fatigue solution. It can also be observed that σ^*_0 does not exert a significant effect on this transitioning of remote stress level from finite to infinite life.

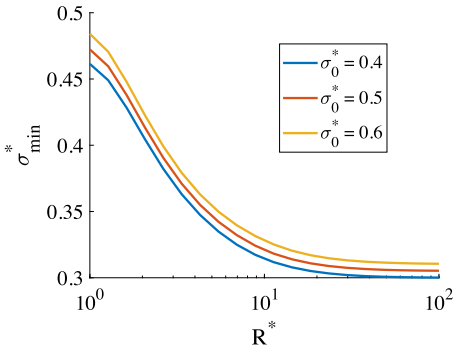

Fig. 8. Minimum remote stress level required for an $a^*_i = 0.3$ crack to grow, as a function of R^*, for different values of σ^*_0.

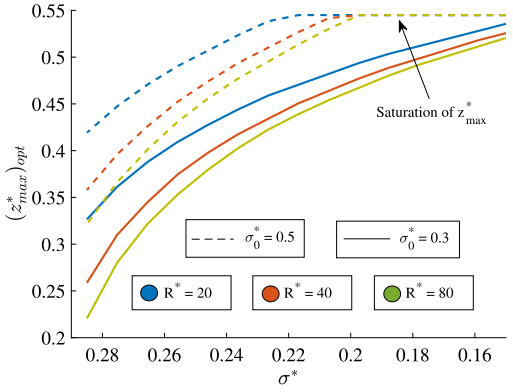

Fig. 9. Infinite life regime solution $(z^*_{max})_{opt}$ in the notch fatigue case, as a function of σ^*, for different values of R^* and σ^*_0.

On the other hand, the infinite life regime depends not only on σ^*_0 (which was the case in a plain fatigue configuration), but also on R^*. This evolution of $(z^*_{max})_{opt}$ when superficial stress level σ^*_0 and notch dimension R^* vary is shown in Fig. 9. Again, a^*_i does not appear in this analysis because no effect of this variable is observed in the infinite life regime, according to Fig. 7. Notice how a small R^* value (approximately less than 10) does not allow for a satisfactory optimization. This happens because the optimal solution for z^*_{max} is found somewhere over $z^*_{max} \approx 0.545$, which is the limit for the consistent region in which the proposed set of parameters can be properly related to the original one, as explained in Appendix A.

6. Conclusions

A new set of parameters $[\sigma_{max}, \sigma_0, z_0, z_{max}]$ for the exponential decay function was proposed. This set of parameters was successfully related to the original one $[A, \lambda, \omega, \theta]$ for a certain range of the new parameters. Particularly, no physically consistent relation could be obtained for values of z^*_{max} greater than approximately 0.545.

A dual optimality criterion has been implemented for the finite-infinite life domains. For those situations in which stress intensity factors would become negative, a SIF minimization algorithm was implemented so as to prevent crack growth to final failure due to

unexpected perturbations. In the case of finite life, the specimen's fatigue crack growth life maximization was taken into consideration.

For every possible situation, the specimen's strength was monotonically increasing with σ_0^*, so it is suggested that this variable be set as high as technically possible. Since optimization with respect to σ_0^* is straightforward, we focus our attention on optimizing the specimen's strength with respect to z_{max}^*.

In the finite life domain for plain fatigue, the optimum value for z_{max}^* was shown to depend almost linearly on a_i^* and slightly on σ^*, but a marginal dependence was found with respect to σ_0^* or the Paris law exponent m. In the infinite life domain for plain fatigue, z_{max}^* is now a function of both σ^* and σ_0^*. No dependence was observed with respect to a_i^*. Paris law exponent m is not present in this particular analysis since no crack growth takes place.

In the case of plain fatigue, the transition from infinite to finite life domain takes place for a remote stress level $\sigma^* \approx 0.95$, and this value was almost independent of every other variable present in the model. This was not the case in the notched situation, where transitioning remote stress level σ^* was shown to depend on the size of the notch, R^*. The finite life domain in the notched specimen showed no difference with respect to the plain fatigue situation. This is explained by the fact that the finite life domain in the notched situation is very restricted (very high loads are required for cracks to grow, considering that we are not allowing any point in the domain to experience inelastic behaviour, excluding the crack tip) and can only take place for very large R^* values, leading to negligible stress gradients in the notch and thus recovering the plain fatigue results (with a factor of 3 for applied stresses, due to stress concentration). In the infinite life domain for the notched specimen, z_{max}^* was observed to depend on σ_0^*, σ^* and R^*. Again, no dependence with respect to a_i^* was observed in this regime.

CRediT authorship contribution statement

S. Aguado-Montero: Data curation, Formal analysis, Methodology, Software, Visualization, Writing – original draft, Writing – review & editing. **J. Vázquez:** Conceptualization, Methodology, Project administration, Supervision, Validation, Writing – review & editing. **C. Navarro:** Methodology, Project administration, Supervision, Validation, Writing – review & editing. **J. Domínguez:** Conceptualization, Project administration, Supervision, Validation, Writing – review & editing.

Declaration of competing interest

The authors declare that they have no known competing financial interests or personal relationships that could have appeared to influence the work reported in this paper.

Appendix A. Relating both sets of parameters in the exponential decay function

The new set of parameters $[z_0, z_{max}, \sigma_0, \sigma_{max}]$ can be mathematically defined in terms of the original set $[A, \lambda, \omega, \theta]$ as follows:

$$\sigma_{res}(0) = \sigma_0 = A\cos(\theta) \tag{A.1}$$

$$\left.\frac{\partial \sigma_{res}}{\partial z}\right|_{z_{max}} = -\lambda A e^{-\lambda z_{max}}\cos(\omega z_{max}+\theta) - \omega A e^{-\lambda z_{max}}\sin(\omega z_{max}+\theta) = 0 \tag{A.2}$$

$$\sigma_{res}(z_{max}) = \sigma_{max} = A e^{-\lambda z_{max}}\cos(\omega z_{max}+\theta) \tag{A.3}$$

$$\sigma_{res}(z_0) = A e^{-\lambda z_0}\cos(\omega z_0+\theta) = 0 \tag{A.4}$$

To derive the nondimensional version of the residual stress profile, the following can be written:

$$\frac{\sigma_{res}}{\sigma_{max}} = \frac{A e^{-\lambda z}\cos(\omega z+\theta)}{A e^{-\lambda z_{max}}\cos(\omega z_{max}+\theta)} \tag{A.5}$$

Additionally, we rewrite some of the terms in the previous expression and define the following nondimensional parameters: $\sigma_{res}^* \equiv \frac{\sigma_{res}}{\sigma_{max}}$, $\lambda^* \equiv \lambda z_0$, $w^* \equiv \omega z_0$, $z^* \equiv \frac{z}{z_0}$, $z_{max}^* \equiv \frac{z_{max}}{z_0}$ and $\sigma_0^* \equiv \frac{\sigma_0}{\sigma_{max}}$.

The following expression is obtained:

$$\sigma_{res}^* = e^{-\lambda^*(z^*-z_{max}^*)}\frac{\cos(\omega^* z^*+\theta)}{\cos(\omega^* z_{max}^*+\theta)} \tag{A.6}$$

which is completely nondimensional. The next step involves relating θ, λ^* and ω^* with the other set of nondimensional parameters.

Eq. (A.4) provides a direct relation between ω^* and θ:

$$\omega^* + \theta = \frac{\pi}{2} \tag{A.7}$$

while Eq. (A.2) governs the relation between λ^* and ω^*:

$$\frac{\lambda}{\omega} = \frac{\lambda^*}{\omega^*} = -\tan(\omega^* z_{max}^* + \theta) \tag{A.8}$$

which can be combined with Eq. (A.7):

$$\lambda^* = -\omega^*\tan^{-1}(\omega^*(1-z_{max}^*)) \tag{A.9}$$

where $\tan^{-1}(x) \equiv \frac{1}{\tan(x)}$ is implied.

Taking Eqs. (A.1) and (A.3) into consideration:

$$\frac{\sigma_0}{\sigma_{max}} = \sigma_0^* = e^{\lambda^* z_{max}^*}\frac{\cos(\theta)}{\cos(\omega^* z_{max}^*+\theta)} \tag{A.10}$$

which is again combined with Eq. (A.7):

$$\sigma_0^* = e^{\lambda^* z_{max}^*}\frac{\sin(\omega^*)}{\sin(\omega^*(1-z_{max}^*))} \tag{A.11}$$

Next, Eqs. (A.9) and (A.11) are combined, yielding an implicit function of ω^* and the nondimensional parameters of interest:

$$\sigma_0^*\frac{\sin(\omega^*(1-z_{max}^*))}{\sin(\omega^*)} - e^{-(\omega^*\tan^{-1}(\omega^*(1-z_{max}^*))z_{max}^*)} = f(\omega^*, \sigma_0^*, z_{max}^*) = 0 \tag{A.12}$$

At this point, Eq. (A.12) yields a value for ω^* provided that σ_0^* and z_{max}^* are fixed. Eqs. (A.7) and (A.9) then allow one to calculate λ^* and θ, respectively. Eq. (A.6) then evaluates the nondimensional residual stress profile at a certain depth.

To solve the implicit ω^* function derived in the previous section, the Newton–Raphson algorithm will be applied. To do so, the function derivative with respect to ω^* needs to be calculated as follows:

$$\begin{aligned}\frac{\partial f}{\partial \omega^*} = {} & z_{max}^*\left[\tan^{-1}(\omega^*(1-z_{max}^*)) - \omega^*\frac{1-z_{max}^*}{\sin^2(\omega^*(1-z_{max}^*))}\right] \\ & \times e^{-(\omega^*\tan^{-1}(\omega^*(1-z_{max}^*))z_{max}^*)} \\ & + \sigma_0^*\left[\cos(\omega^*(1-z_{max}^*))(1-z_{max}^*) - \frac{\sin(\omega^*(1-z_{max}^*))}{\tan(\omega^*)}\right]\frac{1}{\sin(\omega^*)}\end{aligned} \tag{A.13}$$

Additionally, if one closely observes Eq. (A.12), then it can be determined that f is unbounded as $\omega^*(1-z_{max}^*)$ tends to π^-. This can be clearly observed in Fig. A.1. An ω^* value close (from the left) to the critical value is a natural starting point to iterate with the Newton–Raphson algorithm.

Fig. A.2a shows the results obtained with the Newton–Raphson algorithm. For z_{max}^* values higher than 0.545, the Newton–Raphson algorithm does not yield a satisfactory result after the maximum number of iterations is reached. For that reason, we will keep our nondimensional variables within the well-behaved region, i.e. $z_{max}^* < 0.545$. This situation is shown in Fig. A.2b, where a zero valued ω^* region is now observed. This situation is also unrealistic, so once again it will be necessary to avoid it. It is interesting to elucidate the boundary of the allowed region. This can be calculated by computing the limit of f as ω^* tends to zero since this allowed region boundary is a zero ω^* valued curve. L'Hopital's rule was used to compute the limit:

$$\lim_{\omega^*\to 0^+} f(\omega^*, \sigma_0^*, z_{max}^*) = \sigma_0^*(1-z_{max}^*) - e^{-\frac{z_{max}^*}{1-z_{max}^*}} = g(\sigma_0^*, z_{max}^*) = 0 \tag{A.14}$$

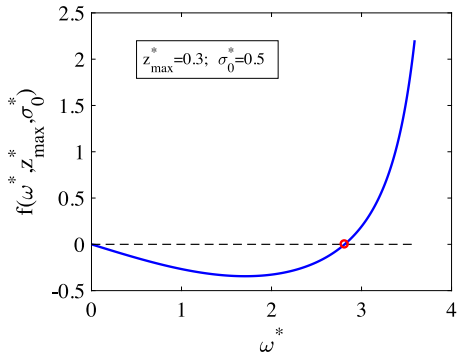

Fig. A.1. Example of implicit f function solved for ω^*.

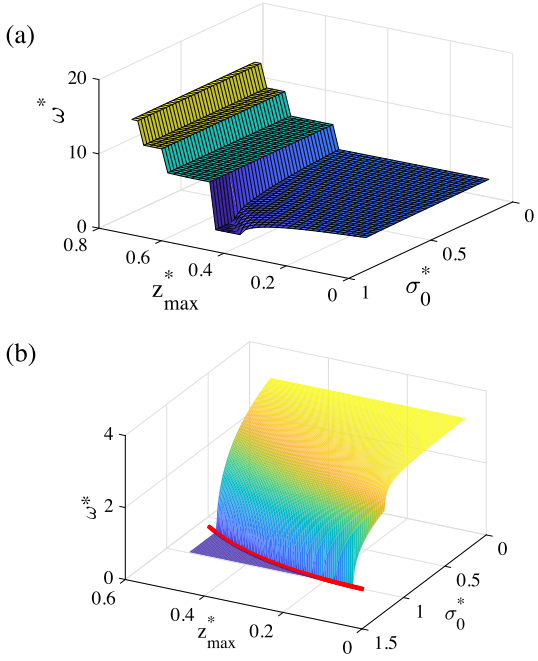

Fig. A.2. (a) ω^* for every possible value for nondimensional parameters z^*_{max} and σ^*_0; (b) ω^* in a more restricted range for z^*_{max}.

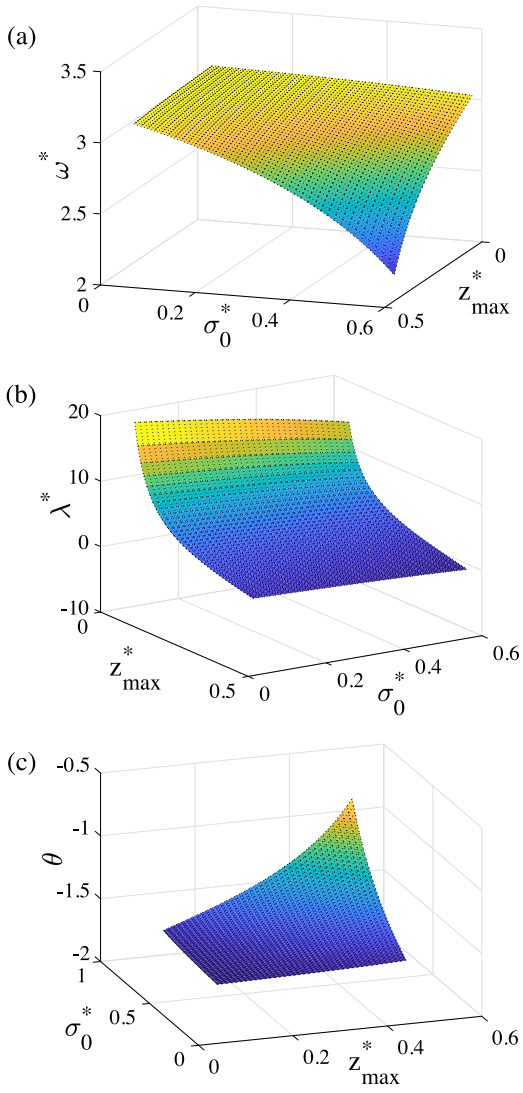

Fig. A.3. (a) ω^*, (b) λ^* and (c) θ as a function of nondimensional parameters z^*_{max} and σ^*_0 in a physically consistent range.

which yields an implicit function of the two nondimensional variables. This curve represents the boundary for the allowed region of analysis, and can be observed in Fig. A.2b. Figs. A.3a, A.3b and A.3c show the final results of translating one set of nondimensional parameters into the other, well within the allowed, physically consistent region bounded by $z^*_{max} = 0.545$ and Eq. (A.14).

Appendix B. Nondimensional analysis of crack growth

Once residual stresses can be evaluated at a certain depth, provided that values for σ^*_0 and z^*_{max} are specified, it is possible to compute mode I stress intensity factors, both associated to residual stresses and to externally applied loads. In both situations, a weight function method will be used in order to establish a systematic procedure which is valid for more general geometries and load configurations:

$$K_{res}(a) = \int_0^a \sigma_{res}(z) w(z,a) dz \tag{B.1}$$

where a is the crack length (considered as a through crack) and $w(z,a)$ is the weight function, which depends on geometry and crack length. As an example, in plain fatigue of a half-plane specimen, the weight function is as follows [9]:

$$w(z,a) = \frac{2}{\sqrt{\pi a(1-(\frac{z}{a})^2)}}(1.3 - 0.3(\frac{z}{a})^{\frac{5}{4}}) \tag{B.2}$$

The weight function for cracks emanating from a circular notch was obtained from [10].

In order to work with nondimensional variables, mode I stress intensity factors will be divided by a reference value: for example, the stress intensity value associated with a uniform normal remote stress σ_{max} applied on a half-plane with a surface through crack of length a:

$$K^*_{res}(a^*) = \frac{K_{res}(a)}{1.12\sigma_{max}\sqrt{\pi a}} = -\int_0^{a^*} \frac{\sigma_{res}(z^*)}{\sigma_{max}} \frac{w(z^*,a^*)}{1.12\sqrt{\pi a}} z_0 \, dz^* \tag{B.3}$$

where the following non-dimensional crack length and weight function definitions are established:

$$a^* \equiv \frac{a}{z_0} \tag{B.4}$$

$$\frac{w(z^*,a^*)}{1.12\sqrt{\pi a}} z_0 \equiv w^*(z^*,a^*) \tag{B.5}$$

resulting in the following nondimensional expression for the mode I stress intensity factor due to the residual stress:

$$K^*_{res}(a^*) = \int_0^{a^*} \sigma^*_{res}(z^*)\ w^*(z^*, a^*)\ dz^* \tag{B.6}$$

The stress intensity factor associated with externally applied loads can be obtained in a similar fashion:

$$K_{applied}(a) = \int_0^{a} \sigma_{applied}(z)\ w(z, a)\ dz \tag{B.7}$$

which can also be nondimensionalized, making use of the following relation:

$$\sigma_{applied}(z) \equiv \sigma_{applied}\ s(z) \tag{B.8}$$

with $s(z)$ being the stress concentration function, depending on position and geometry.

$$K^*_{applied}(a^*) = \int_0^{a^*} \frac{\sigma_{applied}}{\sigma_{max}}\ s(z^*)\ w^*(z^*, a^*)\ dz^* \tag{B.9}$$

Next, fatigue crack growth life can be computed from Paris law integration:

$$\int_0^{N_f} dN = \int_{a_i}^{a_f} \frac{da}{CK^m} \tag{B.10}$$

As we mentioned in a previous section, we consider the main fraction of total fatigue crack growth life to be held within the compressive residual stressed region. For this reason, total compressive region depth, i.e. z_0, is considered as the final integration length. The fraction of fatigue crack growth life from this stage on is considered to be negligible.

Since the aim of the present work is to optimize the residual stress profile applied to a certain specimen, fatigue crack growth life will be nondimensionalized by its value when residual stresses are not present. This means that N^* measures the improvement in fatigue strength due to the presence of a particular residual stress configuration. Fatigue crack growth life is first expressed in terms of nondimensional stress intensity factors:

$$N = \int_{\frac{a_i}{z_0}}^{1} \frac{z_0\ da^*}{C(K^*_{res} + K^*_{applied})^m (1.12\ \sigma_{max}\sqrt{\pi \frac{a}{z_0} z_0})^m} \tag{B.11}$$

If the non-residual-stressed fatigue crack growth life is used to nondimensionalize, then the term $\frac{z_0}{C(1.12\ \sigma_{max}\sqrt{\pi z_0})^m}$ cancels out, yielding:

$$N^* = \frac{\int_{a_i^*}^{1} ((K^*_{res} + K^*_{applied})\sqrt{a^*})^{-m}\ da^*}{\int_{a_i^*}^{1} (K^*_{applied}\sqrt{a^*})^{-m}\ da^*} \tag{B.12}$$

References

[1] W. Renzhi, Effect of residual-stresses of shot peening on the fatigue behavior of a high-strength steel, Fat. Eng. Mater. Struct. 2 (1979) 413–418, http://dx.doi.org/10.1111/j.1460-2695.1979.tb01098.x.

[2] V. Martí n, J. Vázquez, C. Navarro, J. Domí nguez, Fretting-fatigue analysis of shot-peened al 7075-t651 test specimens, Metals (Basel) 9 (2019) 586, http://dx.doi.org/10.3390/met9050586.

[3] V. Martí n, J. Vázquez, C. Navarro, J. Domí nguez, Effect of shot peening residual stresses and surface roughness on fretting fatigue strength of Al 7075-T651, Tribol. Int. 142 (2020) 106004, http://dx.doi.org/10.1016/j.triboint.2019.106004.

[4] J. Vázquez, C. Navarro, J. Domí nguez, Experimental results in fretting fatigue with shot and laser peened Al 7075-T651 specimens, Int. J. Fatigue 40 (2012) 143–153, http://dx.doi.org/10.1016/j.ijfatigue.2011.12.014.

[5] L. Tan, C. Yao, D. Zhang, J. Ren, Empirical modeling of compressive residual stress profile in shot peening TC17 alloy using characteristic parameters and sinusoidal decay function, Proc. Inst. Mech. Eng. Part B J. Eng. Manuf. 232 (2018) 855–866, http://dx.doi.org/10.1177/0954405416657585.

[6] D. Croccolo, L. Cristofolini, M. Bandini, A. Freddi, Fatigue strength of shot-peened nitrided steel: optimization of process parameters by means of design of the experiment, Fatigue Fract. Eng. Mater. Struct. 25 (2002) 695–707, http://dx.doi.org/10.1046/j.1460-2695.2002.00533.x.

[7] X. Wang, Z. Wang, G. Wu, J. Gan, Y. Yang, H. Huang, et al., Combining the finite element method and response surface methodology for optimization of shot peening parameters, Int. J. Fatigue 129 (2019) 105231, http://dx.doi.org/10.1016/j.ijfatigue.2019.105231.

[8] Ulutan D, Y.M. Arisoy, T. Özel, Mears Laine, Empirical modeling of residual stress profile in machining nickel-based superalloys using the sinusoidal decay function. in: Procedia CIRP 2014, 13, 2014, pp. 365–370.

[9] C.M. Sih, Handbook of Stress Intensity Factors, Lehigh University, 1973.

[10] W. Zhao, X.R. Wu, M.G. Yan, Weight function method for three dimensional crack problems—II. Application to surface cracks at a hole in finite thickness plates under stress gradients, Eng. Fract. Mech. 34 (3) (1989) 609–624.